Numerical Study of Ion Beam Evolution by Applying Pulsed Magnetic Field to RF Plasma*)

Takumi MATSUZAWA, Taichi TAKEZAKI and Hiroaki ITO

Faculty of Engineering, University of Toyama, 3190 Gofuku, Toyama 930-8555, Japan

(Received 9 January 2023 / Accepted 29 March 2023)

We numerically investigated the ion behavior in radio frequency (RF) plasma with a pulsed magnetic field applied to a high-current ion source. A one-dimensional hybrid particle-in-cell (PIC) simulation was performed. The numerical results demonstrate the generation process of an ion beam by applying a pulsed magnetic field to the RF plasma. The pulsed magnetic field induces an electric field owing to the interaction between the plasma and the magnetic field. The induced electric field forms a density gradient, and an electrostatic field is generated. The electrostatic field propagates as an ion acoustic wave; some ions in the plasma are accelerated, and an ion beam is generated.

Keywords: RF plasma, ion beam, particle acceleration, pulsed magnetic field, hybrid PIC

DOI: 10.1585/pfr.18.2401044

1. Introduction

Ion beams are used in various scientific and engineering applications, such as material processing and energy drivers for fusion reactors [1–4]. Ion sources generate and provide seed ions for ion beams, and are expected to increase the beam current density toward high power and improve the processing efficiency.

In conventional ion sources using radio frequency (RF) plasma, the plasma is generated by gas discharge, and ion beams are extracted by applying a high voltage to the plasma. In this process, the charge neutrality of the plasma is broken, and the extracted beam current density is imposed by the space-charge-limited current (Child-Langmuir current) and Bohm current [2,5]. To avoid these limitations, a novel mechanism for transporting and accelerating ion beams while maintaining the charge neutrality of the plasma is required.

Beam generation while maintaining charge neutrality is a phenomenon observed in astrophysics owing to the nonlinear interactions between the plasma and the magnetic field. Non-thermal high-energy particles exist in outer space [6] and are generated by the interactions, such as collisionless shocks, between the plasma flow and electromagnetic fields. To elucidate the generation mechanisms for non-thermal particles, laboratory-scale experiments and numerical simulations have been performed [7–12]. Particle-in-cell (PIC) simulations of high-power laser experiments have predicted the formation of electrostatic collisionless shocks and generation of reflected ion beams at the shock surface [9,10]. Moreover, a laboratory-scale experiment using pulsed-power discharge and its numerical simulations have demonstrated the generation of accelerated ions caused by the interaction between a fast plasma flow and perpendicular magnetic field [11,12].

Laboratory-scale experiments using high-power lasers [7,8] and pulsed-power discharges [11] have generated a fast plasma flow that evolves in interaction with a steady magnetic field. To apply the nonthermal particle generation process discussed in astrophysics to RF plasma, a time-evolving magnetic field should be applied to the steady plasma. Several studies on RF plasma dynamics have applied steady magnetic fields, such as in plasma thrusters, and significantly contributed to plasma physics [13]. In recent years, experiments applying an axial pulsed magnetic field to an RF plasma thruster have been reported, and new theories in plasma physics have been developed [14]. Steady plasmas, such as the RF plasma, exhibit good reproducibility and detailed plasma diagnostics, and are thus expected to contribute to space plasma physics and astrophysics. In this study, we numerically investigated the ion behavior in RF plasma by applying a pulsed magnetic field. A one-dimensional hybrid PIC simulation was performed to investigate the beam behavior of the ions.

2. Setup of Numerical Simulation

To calculate the ion particle motion in the RF plasma, we used a hybrid PIC method [11, 12, 15]. Owing to the mass difference between ions and electrons, electrons were treated as a massless fluid that immediately satisfied the charge neutrality in the hybrid PIC. Therefore, the spatial and temporal scales of the analysis were determined based on the scale of the ion motion, and the computational cost of the hybrid PIC method was lower than that of the full

author's e-mail: m22c1492@ems.u-toyama.ac.jp, takezaki@eng.u-toyama.ac.jp

*) This article is based on the presentation at the 31st International Toki Conference on Plasma and Fusion Research (ITC31).

PIC method. Moreover, because the ions are treated as particles, the hybrid PIC enables the discussion of nonthermal beam effects, which cannot be discussed in magnetohydrodynamic simulations.

The equations of motion for the ions treated as particles are described as follows:

$$\frac{d\boldsymbol{x}_p}{dt} = \boldsymbol{v}_p, \tag{1}$$

$$m_p \frac{d\boldsymbol{v}_p}{dt} Ze(\boldsymbol{E} + \boldsymbol{v}_p \times \boldsymbol{B}), \tag{2}$$

where $\boldsymbol{x}_p$ is the ion position, $\boldsymbol{v}_p$ is the ion velocity, m_p is the ion mass, Z is the ion charge state, e is the elementary charge, $\boldsymbol{E}$ is the electric field, and $\boldsymbol{B}$ is the magnetic field. The electron fluid and electromagnetic field are expressed as follows:

$$\boldsymbol{u}_e = \boldsymbol{u}_p - \frac{\nabla \times \boldsymbol{B}_p}{\mu_0 e n_e}, \tag{3}$$

$$n_e = Z n_p, \tag{4}$$

$$P_e = n_e k_B T_e, \tag{5}$$

$$P_e n_e^{-\gamma} = \text{constant}, \tag{6}$$

$$\boldsymbol{E} = -\boldsymbol{u}_e \times \boldsymbol{B} - \frac{\nabla P_e}{e n_e}, \tag{7}$$

$$\frac{\partial \boldsymbol{B}_p}{\partial t} = -\nabla \times \boldsymbol{E}, \tag{8}$$

$$\boldsymbol{B} = \boldsymbol{B}_p + \boldsymbol{B}_0, \tag{9}$$

where $\boldsymbol{u}_p$ and $\boldsymbol{u}_e$ are the flow velocities of ions and electrons, respectively; n_p and n_e are the number densities of ions and electrons, respectively; P_e is the electron pressure; T_e is electron temperature; $\boldsymbol{B}_p$ and $\boldsymbol{B}_0$ are the induced and external magnetic fields, respectively; μ_0 is the permeability in a vacuum; k_B is the Boltzmann constant, and γ is the adiabatic constant.

The analysis was performed in a one-dimensional space (x) with three velocity dimensions (v_x, v_y, v_z). The analytical model is shown in Fig. 1. The calculation region was set to 100 mm. Superparticles representing argon ions with a charge state $Z = 1$ were randomly placed in the region from $x = -100$ mm to $x = 200$ mm, and the particles could move freely at the boundaries both upstream and downstream. The plasma parameters were set to typical RF plasma values as follows [16]: number density $n_p = n_e = 10^{19}\,\mathrm{m}^{-3}$, ion temperature $T_p = 0.1$ eV, electron temperature $T_e = 3$ eV, and drift velocity $v_d = 2.5$ km/s.

A pulsed external magnetic field with a Gaussian distribution with a peak of 10 mT at $x = 40$ mm and a half-period of 4 μs was applied to the RF plasma. The field parameters were determined based on the specifications of the developed pulsed magnetic field generator. For both upstream and downstream boundary conditions the electromagnetic fields at the boundaries were set to zero throughout the analysis. The calculation was completed before the effect of the boundaries affected the ion behavior.

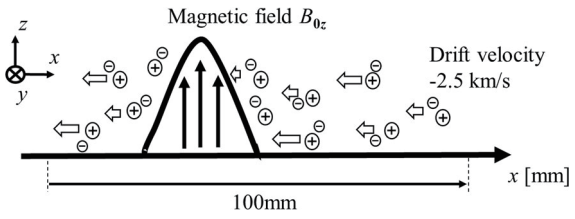

Fig. 1 Analytical model.

3. Results and Discussion

Figure 2 shows the time evolution of the x-v_x ion phase space, ion number density n_p, electric field E_x, and magnetic field B_z. In the initial stage of the analysis, the plasma flowed in the $-x$ direction owing to drift velocity. By applying a pulsed magnetic field, some ions were accelerated in the $+x$ direction, and an ion beam was generated.

The spatial distribution of the ion number density at $t = 2$ and 4 μs, as shown in Figs. 2 (a) and 2 (b), indicates the increase of the density upstream of the pulsed magnetic field. Because the plasma flow is prevented by a pulsed magnetic field, the plasma stagnates near the peak of the magnetic field, forming a density gradient. The time evolution of the magnetic field shows a change in the spatial distribution of the pulsed magnetic field. As the plasma flow compressed the magnetic field, the spatial gradient of the magnetic field became steeper.

At $t = 8$ μs, as shown in Fig. 2 (c), the density gradient formed at the beginning of the analysis propagates in the $+x$ direction. Moreover, the ion beam continued to be generated during the propagation of the density gradient, after the duration of the pulse, and outside the applied region of the pulsed magnetic field. The electric field $\boldsymbol{E}$ shown in Eq. (7) can be approximated in the x direction as follows:

$$E_x \approx -\frac{B_z}{\mu_0 e n_e}\frac{\partial B_z}{\partial x} - \frac{1}{e n_e}\frac{\partial P_e}{\partial x}. \tag{10}$$

The first term on the right side of Eq. (10) represents the induced electric field generated by the spatial gradient of the magnetic field, and the second term represents the electrostatic field caused by the electron pressure gradient. In the initial stage of the analysis, the induced electric field is generated, increasing the density gradient. The electron pressure gradient term also indicates the gradient of the ion number density from Eqs. (4) - (6). As shown in Fig. 2 (c), the ion density gradient corresponds to the electric field that acts as a source for generating the ion beam. Figure 3 shows the results obtained by neglecting the effect of electron pressure.

Although the ion beam was initially generated, the density gradient and electric field did not propagate, and the velocity of the ions rapidly decayed. This indicates that the electrostatic field contributed to generating the ion beam after the pulse duration and outside the applied region of the magnetic field.

Figure 4 shows the space-time evolution of the electric field E_x. The electric field propagated at an almost constant

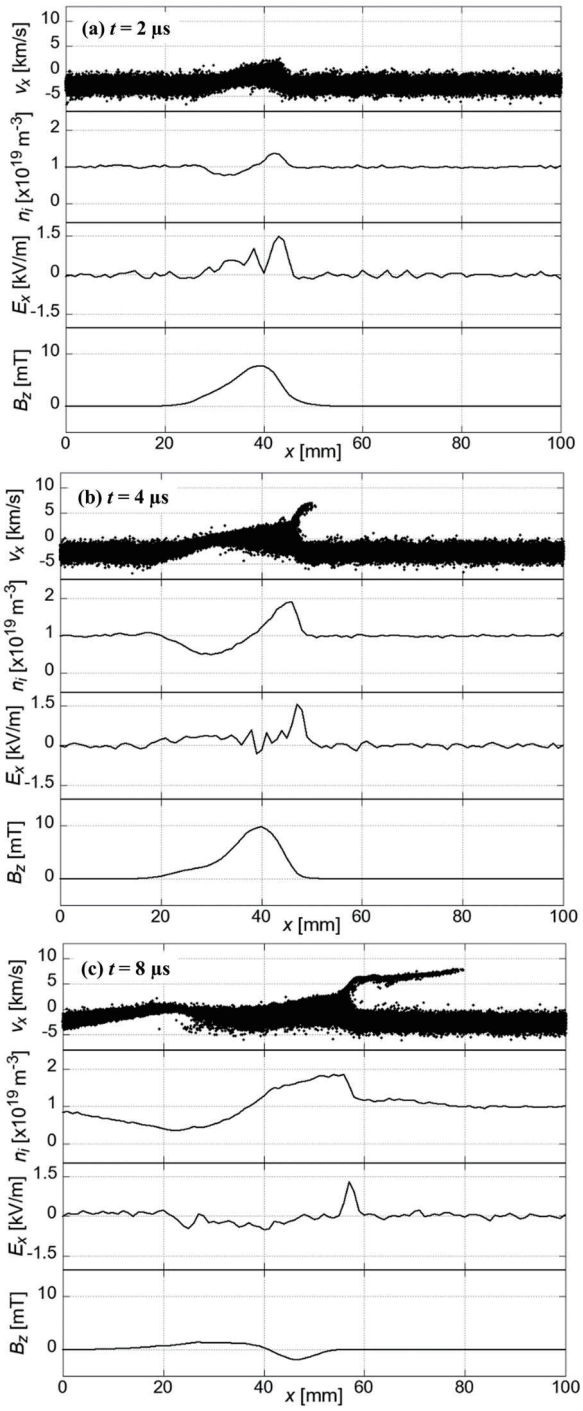

Fig. 2 Time evolution of the ion x-v_x phase space, ion number density, and electromagnetic fields at a) $t = 2\,\mu$s, b) $t = 4\,\mu$s, and c) $t = 8\,\mu$s.

velocity of 2.6 km/s. The ion acoustic speed is expressed as follows [5]:

$$v_s = \left(\frac{k_B T_e + \gamma k_B T_p}{m_p} \right)^{1/2}. \tag{11}$$

Using the calculated values, the ion acoustic speed was estimated as $v_s = 2.69$ km/s. The propagation velocity of the electric field shown in Fig. 4 was approximately equal to

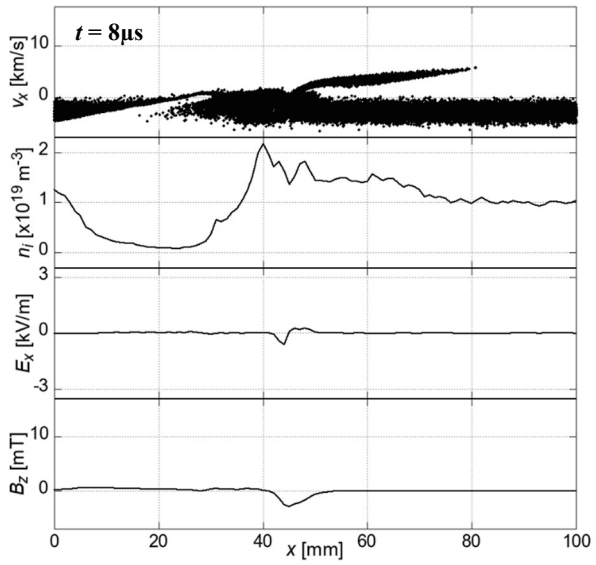

Fig. 3 Numerical result of artificially neglecting the electron pressure.

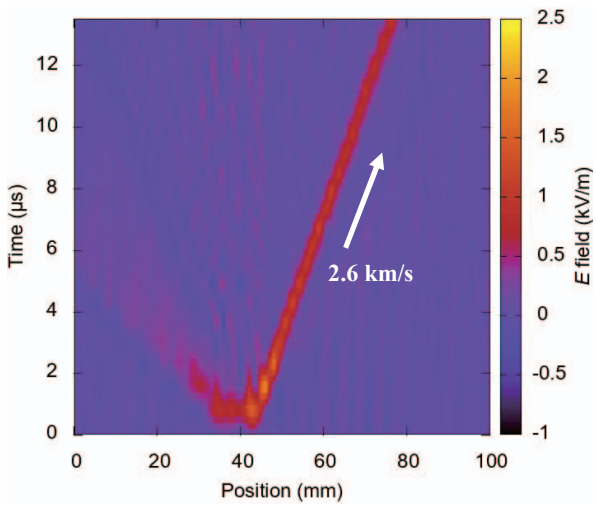

Fig. 4 Space-time evolution of the electric field E_x.

the ion acoustic speed. This indicated that the electrostatic field propagated as an ion acoustic wave.

4. Conclusion

In this study, we performed a numerical simulation based on the hybrid PIC method to investigate the ion behavior in RF plasma with an applied pulsed magnetic field. The numerical results demonstrated the ion beam generation process by applying a pulsed magnetic field to the RF plasma. The plasma flow stagnated when a pulsed magnetic field was applied, and a gradient of density and magnetic field were formed. These gradients generated an electric field, and some ions in the RF plasma were accelerated. The electric field consisted of the induced electric field caused by the gradient of the magnetic field and electrostatic field caused by the density gradient. The induced

electric field forms a density gradient, and the electrostatic field propagates as an ion acoustic wave and generates an ion beam. In the future, we will experimentally and numerically investigate the effects of the peak value, half-period, and spatial distribution of the pulsed magnetic field on the ion behavior.

Acknowledgments

This work was partly supported by Charitable Trust Ame Hisaharu Universities Research Grant Fund.

[1] J. Ishikawa, Rev. Sci. Instrum. **71**, 1036 (2000).
[2] A. Anders, Surf. Coat. Technol. **200**, 1893 (2005).
[3] M. Okamura, A. Adeyemi, T. Kanesue, J. Tamura, K. Kondo and R. Dabrowski, Rev. Sci. Instrum. **81**, 02A510 (2010).
[4] M.M. Abdelrahman, J. Phys. Sci. Appl. **5**, 128 (2015).
[5] F.F. Chen, *Introduction to Plasma Physics and Controlled Fusion*, 3rd ed. (Springer, 2016).
[6] S. Swordy, in *The Astrophysics of Galactic Cosmic Rays* (Springer, 2001), pp. 85-94.
[7] R. Yamazaki, S. Matsukiyo, T. Morita, S.J. Tanaka, T. Umeda, K. Aihara, M. Edamoto, S. Egashira, R. Hatsuyama, T. Higuchi *et al.*, Phys. Rev. E **105**, 025203 (2022).
[8] S. Matsukiyo, R. Yamazaki, T. Morita, K. Tomita, Y. Kuramitsu, T. Sano, S.J. Tanaka, T. Takezaki, S. Isayama, T. Higuchi *et al.*, Phys. Rev. E **106**, 025205 (2022).
[9] R. Kumar, Y. Sakawa, T. Sano, L.N. Döhl, N. Woolsey and A. Morace, Phys. Rev. E **103**, 043201 (2021).
[10] Y. Sakawa, Y. Ohira, R. Kumar, A. Morace, L.N. Döhl and N. Woolsey, Phys. Rev. E **104**, 055202 (2021).
[11] T. Takezaki, K. Kakinuma, Y. Shikuma, K. Takahashi, T. Sasaki, T. Kikuchi and N. Harada, High Energy Density Phys. **33**, 100698 (2019).
[12] T. Takezaki, S. Kato, T. Oguchi, S. Watanabe, K. Takahashi, T. Sasaki, T. Kikuchi and H. Ito, Phys. Plasmas **28**, 102109 (2021).
[13] K. Takahashi, Rev. Mod. Plasma Phys. **3**, 3 (2019).
[14] H. Sekine, H. Koizumi and K. Komurasaki, AIP Advances **11**, 015102 (2021).
[15] D. Winske, L. Yin, N. Omidi, H. Karimabadi and K. Quest, in *Space Plasma Simulation* (Springer, 2003), pp. 136 - 165.
[16] K. Toki, S. Shinohara, T. Tanikawa and K. P. Shamrai, Thin Solid Films **506-507**, 597 (2006).